



CHORUS

This is the accepted manuscript made available via CHORUS. The article has been published as:

Time-Resolved Measurements of Hot-Electron Equilibration Dynamics in High-Intensity Laser Interactions with Thin-Foil Solid Targets

P. M. Nilson, J. R. Davies, W. Theobald, P. A. Jaanimagi, C. Mileham, R. K. Jungquist, C. Stoeckl, I. A. Begishev, A. A. Solodov, J. F. Myatt, J. D. Zuegel, T. C. Sangster, R. Betti, and D. D. Meyerhofer

Phys. Rev. Lett. **108**, 085002 — Published 22 February 2012

DOI: [10.1103/PhysRevLett.108.085002](https://doi.org/10.1103/PhysRevLett.108.085002)

**Time-Resolved Measurements of Hot-Electron Equilibration Dynamics in
High-Intensity Laser Interactions with Thin-Foil Solid Targets**

P. M. Nilson^{1,2}, J. R. Davies^{1,2,3}, W. Theobald², P. A. Jaanimagi², C. Mileham²,
R. K. Jungquist², C. Stoeckl², I. A. Begishev², A. A. Solodov^{1,2}, J. F. Myatt²,
J. D. Zuegel², T. C. Sangster², R. Betti^{1,2,3}, and D. D. Meyerhofer^{1,2,3}

¹Fusion Science Center for Extreme States of Matter and Fast Ignition Physics,
University of Rochester, Rochester, NY

²Laboratory for Laser Energetics, University of Rochester

³also Depts. of Mechanical Engineering and Physics, University of Rochester

Time-resolved K_{α} spectroscopy has been used to infer the hot-electron equilibration dynamics in high-intensity laser interactions with picosecond pulses and thin-foil solid targets. The measured K_{α} -emission pulse width increases from ~ 3 to 6 ps for laser intensities from $\sim 10^{18}$ to 10^{19} W/cm². Collisional energy-transfer model calculations suggest that hot electrons with mean energies from ~ 0.8 to 2 MeV are contained inside the target. The inferred mean hot-electron energies are broadly consistent with ponderomotive scaling over the relevant intensity range.

High-intensity laser interactions with solid targets generate extreme states of matter [1] with unique energy-transport properties [2,3]. At laser intensities above 10^{18} W/cm², high-current electron beams with \sim MeV energies are generated [4–7], heating matter to high thermal temperatures over picosecond time scales [2,3,8]. Understanding the energy partition and its evolution in these highly nonequilibrium plasmas is an important open issue, underpinning applications in high-energy-density science [1], plasma-based particle acceleration [9], warm dense matter [10], high-peak-power γ -ray generation [11], and advanced inertial fusion energy concepts, including fast ignition [12]. In these conditions, the hot-electron equilibration dynamics are not completely understood and accurate time-resolved measurements are required to test energy partition and temperature equilibration models.

The only previous hot-electron equilibration data in this regime are the time-resolved K_{α} -emission data of Chen *et al.* [13]. Those experiments irradiated thin-foil targets with \sim 0.5-ps pulses focused to intensities up to 10^{19} W/cm² and used the K_{α} -emission pulse width to characterize the time scale for energy thermalization (“relaxation”) between hot and cold electrons. The data showed K_{α} -emission pulse widths from \sim 12 to 16 ps. The data were compared to an electron-energy transfer model that included ion-front expansion and collisional electron-energy transfer based on Landau–Spitzer theory [14]. With increasing laser intensity, the model did not reproduce the rise time (\sim 10 ps) or the duration of the measured K_{α} signals, revealing an incomplete picture of the hot-electron equilibration dynamics.

In this Letter, ultrafast measurements of the hot-electron relaxation time in high-intensity laser-solid interactions are reported. Thin-foil targets were irradiated with 0.5- to 1-ps pulses focused to intensities from $\sim 10^{18}$ to 10^{19} W/cm² and the hot-electron equilibration dynamics studied with time-resolved K_{α} spectroscopy. In these interactions, the full width at half maximum (FWHM) of the K_{α} signal increases with laser intensity from ~ 3 to 6 ps. These are the first experiments at relativistic laser intensities to show rapid hot-electron relaxation times with K_{α} -emission pulse widths up to a factor of 4 \times shorter than in previously reported experiments [13]. To provide insight into the mean energy of the hot electrons contained inside the target, the duration of the measured K_{α} signals are compared to predictions from a collisional energy-transfer model. Assuming collisional energy transfer dominates, the data suggest that hot electrons with mean energies from ~ 0.8 to 2 MeV are contained inside the target. The inferred mean hot-electron energies are broadly consistent with ponderomotive scaling [6] over the relevant intensity range.

The experiments were carried out with the Multi-Terawatt (MTW) laser [15] at the University of Rochester's Laboratory for Laser Energetics. Figure 1 shows a schematic of the experimental setup. The MTW laser delivered 1- to 10-J, 0.5- to 1-ps pulses at a wavelength of $1.053 \mu\text{m}$ that were focused by an $f/3$ off-axis parabolic mirror to a spot with a FWHM of $\sim 5 \mu\text{m}$, providing peak vacuum-focused intensities from $\sim 10^{18}$ to 10^{19} W/cm². The laser-intensity contrast was $\sim 10^8$ at 100 ps before the peak of the main laser pulse [16]. The laser was focused at normal incidence on $500 \times 500 \times 20\text{-}\mu\text{m}^3$ Cu-foil targets mounted on $17\text{-}\mu\text{m}$ -diam silicon carbide stalks.

Time resolving the K_{α} radiation generated in these experiments is a direct technique for inferring the hot-electron relaxation time [13]. K_{α} radiation emitted from the target was measured with a 2-ps time-resolution x-ray streak camera [17] coupled to a HAPG (highly annealed pyrolytic graphite) crystal spectrometer. The HAPG crystal was $50 \times 14 \text{ mm}^2$ in area and had a three dimensional, elliptically curved surface with radii $R_1 = -22.000 \text{ mm}$ and $R_2 = -10.620 \text{ mm}$, and conic constants $k_1 = -0.825$ and $k_2 = -0.955$ mm, collecting radiation from 7.8 to 8.5 keV. This spectral range covers the $2p \rightarrow 1s$ transition in Cu, allowing for time-resolved Cu K_{α} measurements at 8.05 keV.

The streak camera was independently characterized by direct illumination of the photocathode with a 10-mJ, 0.5-ps pulse of 263-nm light. Figure 2 shows a schematic of the setup. By passing half of the UV beam through a quartz plate of known thickness, two pulses were generated, providing a sweep-speed calibration. Figure 2(b) shows a typical streak-camera trace for these two pulses. The pulse widths (FWHM) are 1.8 ± 0.1 and 1.9 ± 0.1 ps. Temporal dispersion in the streak camera gives a slightly different impulse response for x-ray illumination. Monte Carlo modeling of the electron optics inside the streak tube shows that this offset is ~ 0.2 ps, giving an impulse response for x rays of ~ 2 ps.

Figure 3 shows an example of time-resolved plasma x-ray emission data for different high-intensity laser irradiation conditions. Figure 3(a) shows the time-resolved K_{α} emission from a $500 \times 500 \times 20\text{-}\mu\text{m}^3$ Cu foil irradiated with a 0.9-J, 0.6-ps pulse focused to $3.6 \times 10^{18} \text{ W/cm}^2$. The pulse width is 3.0 ± 0.2 ps. Figure 3(b) shows the K_{α} emission from a similar target irradiated with an 8.5-J, 0.8-ps pulse focused to $2.9 \times$

10^{19} W/cm². The pulse width is 5.5 ± 0.1 ps. The K_α emission from these targets was measured as a peaked signal with a sharp rise and a slower decay. The signal rise time did not vary with laser intensity and was determined by the experimental resolution. The signal decay time increased with laser intensity and was sensitive to the hot-electron equilibration dynamics.

K_α radiation is generated in these experiments by hot electrons that are confined by target charging [7,18,19]. The thin-foil target rapidly charges because of the electrostatic potential that develops after the initial loss of a small fraction of high-energy electrons [18]. The remaining hot electrons (>90% of the total laser-accelerated population) make multiple round-trips of the target as they recirculate (reflux) because their collisional range is several hundred microns at solid density [20].

A collisional energy-loss model for understanding hot-electron relaxation and the time dependence of K_α emission in these targets has been developed. The model calculates the K_α emission rate for a given hot-electron energy distribution, assuming that all of the electrons are trapped inside the foil. The hot-electron energy loss rate is given by [20]

$$\frac{dE}{dt} = -\frac{n_e e^4 L_d}{4\pi\epsilon_0^2 m_e v}, \quad (1)$$

where n_e is the electron density for solid Cu (2.46×10^{24} cm⁻³), E is the hot-electron energy, m_e is the electron rest mass, v is the hot-electron velocity, e is the electron

charge, and ϵ_0 is the permittivity of free space. The stopping number L_d (or “log Λ ”) depends weakly on material and the hot-electron energy, with values for Cu taken from Ref. 21. The time spent by hot electrons outside the target during recirculation is assumed negligible and energy losses to ion acceleration and self-generated electric fields are not considered in this model [7,18,19]. The implications for these assumptions on the inferred mean hot-electron energy will be discussed later.

K_α -emission pulse widths have been calculated for hot electrons with exponential $\left(f_h \propto e^{-\gamma m_e c^2 / k_B T_h} \right)$ and three-dimensional relativistic Maxwellian $\left[f_h \propto \gamma (\gamma^2 - 1)^{1/2} e^{-\gamma m_e c^2 / k_B T_h} \right]$ energy distributions, where f_h is the hot-electron energy distribution function, k_B is Boltzmann’s constant, T_h is the hot-electron temperature, and γ is the Lorentz factor. Isochoric energy transfer to solid matter in these calculations is assumed. The K_α emission rate is proportional to the Cu-ion density, the time-varying number of hot electrons, and the parameter $\langle \sigma_K v \rangle$ averaged over the hot-electron energy distribution, where σ_K is the K-shell ionization cross section and v is the hot-electron velocity. On the timescale of the detection, the conversion of hot-electron energy to a K_α photon is considered to be instantaneous. The cross section for ionization of K-shell electrons was taken from Ref. 21.

Figure 3 shows synthetic K_α streaks that were calculated from this model. The synthetic pulse widths were fit to the data by adjusting the signal intensity and the mean hot-electron energy in the model. They represent a convolution of the calculated K_α -

emission rate with the laser pulse duration and the temporal resolution of the x-ray streak camera. In the low-intensity case [Fig. 3(a)], the model predicts well the K_{α} emission pulse shape, independent of the hot-electron energy distribution that was used. The best fit of the experimental data was obtained with the parameters $\langle E \rangle_{\text{exp}} = 0.47$ MeV for the exponential energy distribution and $\langle E \rangle_{\text{RM}} = 0.58$ MeV for the 3-D relativistic Maxwellian energy distribution. In the high-intensity case [Fig. 3(b)], the best fit was obtained with the parameters $\langle E \rangle_{\text{exp}} = 1.55$ MeV and $\langle E \rangle_{\text{RM}} = 1.73$ MeV. In this case, the K_{α} -emission pulse shape was better reproduced by model calculations with a 3-D relativistic Maxwellian energy distribution.

Figure 4 shows the variation with increasing laser intensity of the measured K_{α} emission pulse width. An upper estimate of the true K_{α} -emission pulse width was obtained by accounting for instrumental effects, subtracting the FWHM of the impulse response function from the streak-camera trace in quadrature. Gaussian pulse shapes are assumed. For laser intensities between 2.7×10^{18} and 3.4×10^{19} W/cm², the duration of the measured K_{α} signal increases from ~ 3 to 6 ps. Over this intensity range, a least squares fit shows that the K_{α} -emission pulse width increases with laser intensity and is given by $\tau_{K_{\alpha}} [\text{ps}] = (4.1 \pm 0.3) I_{19}^{0.35 \pm 0.07}$, where I_{19} is the laser intensity in units of 10^{19} W/cm².

To obtain a mean hot-electron energy scaling, these data were compared with the collisional energy-loss model. Figure 5(a) shows the relationship between the calculated K_{α} -emission pulse width and the mean hot-electron energy for exponential and 3-D

relativistic Maxwellian energy distributions. In these calculations, the K_{α} -emission rate was convolved with a 0.8-ps FWHM Gaussian pulse that approximated the range of laser pulse durations that were used in these experiments. The synthetic pulse was convolved with a 2-ps FWHM Gaussian instrument response that was removed in quadrature for comparison with the experimental data (Fig. 4). Figure 5(a) shows that calculations with a 3-D relativistic Maxwellian energy distribution have slightly higher mean hot-electron energies than with an exponential energy distribution for a given K_{α} emission pulse width. This offset is ~ 100 to 200 keV.

Figure 5(b) shows the mean hot-electron energies that are inferred from the experimental data based on this model. Two scaling laws are obtained: For an exponential energy distribution, $\langle E \rangle_{\text{exp}} [\text{MeV}] = (1.12 \pm 0.11) I_{19}^{0.51 \pm 0.11}$. For a 3-D relativistic Maxwellian energy distribution, $\langle E \rangle_{\text{RM}} [\text{MeV}] = (1.19 \pm 0.11) I_{19}^{0.46 \pm 0.10}$. Assuming collisional energy transfer dominates, these results show that mean hot-electron energies from ~ 0.8 to 2 MeV are required to generate K_{α} -emission pulse widths consistent with the experimental observations.

Figure 5(c) compares these inferred mean hot-electron energies with ponderomotive scaling [6]. Ponderomotive scaling gives

$$\langle E \rangle = m_e c^2 \left[1 + \left(2U_P / m_e c^2 \right) \right]^{1/2}, \text{ where } U_P = 9.33 \times 10^{-14} I [\text{W/cm}^2] \lambda [\mu\text{m}]^2 \text{ is the}$$

ponderomotive potential. In each case, the inferred mean energies are slightly higher compared with ponderomotive scaling. The best agreement was found for calculations with an exponential energy distribution. A similar scaling predicting ~ 100 to 200 keV

higher mean hot-electron energies was found with calculations using the 3-D relativistic Maxwellian energy distribution. Compared with ponderomotive scaling, the power law fits give a faster increase in mean energy with intensity near 10^{18} W/cm² and provide a better fit to the experimental data.

The collisional energy-loss model presented here is not intended to fully model the experiment but is used to help interpret the data. The model neglects energy loss to self-generated electric fields and to ion acceleration and it neglects the time electrons take to be reflected by the electrostatic field outside the target. All of these effects would be expected to increase with laser intensity and an accurate assessment of them will require numerical modeling. The accuracy with which the collisional model reproduces all of the experimental results and the relative insensitivity of the mean energy to the energy distribution indicates that the values are likely not significantly in error. Measurements of the ion emission at these intensities show that it is not a significant energy sink [22]. The results presented here form a comprehensive test bed for future comparison with numerical modeling that may include these effects.

In summary, the hot-electron equilibration dynamics in thin-foil solid targets irradiated with high-intensity laser pulses have been studied. Time-resolved K_{α} spectroscopy measurements show K_{α} -emission pulse widths from ~ 3 to 6 ps for laser intensities between $\sim 10^{18}$ and 10^{19} W/cm². Assuming collisional energy transfer dominates, the experimental data suggest that hot electrons with mean energies from ~ 0.8 to 2 MeV are contained inside the target. The inferred mean hot-electron energy scaling with laser intensity is broadly consistent with ponderomotive scaling. These

findings are important for the understanding of a wide range of high-energy-density physics applications that require a large and fast energy input into matter.

This work was supported by the U.S. Department of Energy Office of Inertial Confinement Fusion under Cooperative Agreement No. DE-FC52-08NA28302, the University of Rochester, and the New York State Energy Research and Development Authority. The support of DOE does not constitute an endorsement by DOE of the views expressed in this article.

References

1. B. A. Remington *et al.*, *Science* **284**, 1488 (1999).
2. J. A. Koch *et al.*, *Phys. Rev. E* **65**, 016410 (2001); K. Eidmann *et al.*, *J. Quant. Spectrosc. Radiat. Transf.* **81**, 133 (2003); P. Audebert *et al.*, *Phys. Rev. Lett.* **94**, 025004 (2005).
3. C. R. D. Brown *et al.*, *Phys. Rev. Lett.* **106**, 185003 (2011).
4. D. F. Price *et al.*, *Phys. Rev. Lett.* **75**, 252 (1995); H. Chen *et al.*, *Phys. Rev. Lett.* **70**, 3431 (1993); K. B. Wharton *et al.*, *Phys. Rev. Lett.* **81**, 822 (1998); K. Yasuike *et al.*, *Rev. Sci. Instrum.* **72**, 1236 (2001); S. P. Hatchett *et al.*, *Phys. Plasmas* **7**, 2076 (2000).
5. F. N. Beg *et al.*, *Phys. Plasmas* **4**, 447 (1997).
6. S. C. Wilks *et al.*, *Phys. Rev. Lett.* **69**, 1383 (1992).
7. P. M. Nilson *et al.*, *Phys. Rev. Lett.* **105**, 235001 (2010).
8. A. Saemann *et al.*, *Phys. Rev. Lett.* **82**, 4843 (1999); P. Audebert *et al.*, *Phys. Rev. Lett.* **89**, 265001 (2002).
9. E. L. Clark *et al.*, *Phys. Rev. Lett.* **84**, 670 (2000); R. A. Snavely *et al.*, *Phys. Rev. Lett.* **85**, 2945 (2000).
10. P. K. Patel *et al.*, *Phys. Rev. Lett.* **91**, 125004 (2003).
11. P. A. Norreys *et al.*, *Phys. Plasmas* **6**, 2150 (1999).
12. M. H. Key *et al.*, *Phys. Plasmas* **5**, 1966 (1998); M. Tabak *et al.*, *Phys. Plasmas* **1**, 1626 (1994).
13. H. Chen *et al.*, *Phys. Rev. E* **76**, 056402 (2007).

14. L. D. Landau, *Phys. Z. Sowjetunion* **10**, 154 (1936); L. Spitzer, *Physics of Fully Ionized Gases*, 2nd rev. ed., Interscience Tracts on Physics and Astronomy (Wiley Interscience, New York, 1962).
15. V. Bagnoud *et al.*, *Opt. Lett.* **30**, 1843 (2005).
16. V. Bagnoud *et al.*, *Opt. Express* **15**, 5504 (2007).
17. C. Stoeckl *et al.*, *Bull. Am. Phys. Soc.* **52**, 67 (2007).
18. J. Myatt *et al.*, *Phys. Plasmas* **14**, 056301 (2007).
19. A. J. Mackinnon *et al.*, *Phys. Rev. Lett.* **88**, 215006 (2002); Y. Sentoku *et al.*, *Phys. Plasmas* **10**, 2009 (2003); W. Theobald *et al.*, *Phys. Plasmas* **13**, 043102 (2006); S. D. Baton *et al.*, *High Energy Density Phys.* **3**, 358 (2007); P. M. Nilson *et al.*, *Phys. Plasmas* **15**, 056308 (2008); P. M. Nilson *et al.*, *Phys. Rev. E* **79**, 016406 (2009).
20. H. O. Wyckoff, *ICRU Report*, International Commission on Radiation Units and Measurements, Inc., Bethesda, MD (1984).
21. J. P. Santos, F. Parente, and Y.-K. Kim, *J. Phys. B:At. Mol. Opt. Phys.* **36**, 4211 (2003); <http://physics.nist.gov/PhysRefData/Star/Test/ESTAR.html>.
22. L. Robson, P. T. Simpson, R. J. Clarke, K. W. D. Ledingham, F. Lindau, O. Lundh, T. McCanny, P. Mora, D. Neely, C.-G. Wahlström, M. Zepf, and P. McKenna, *Nat. Phys.* **3**, 58 (2007); J. Fuchs, P. Antici, E. D'Humières, E. Lefebvre, M. Borchesi, E. Brambrink, C. A. Cacchetti, M. Kaluza, V. Malka, M. Manclossi, S. Meyroneinc, P. Mora, J. Schreiber, T. Toncian, H. Pépin, and P. Audebert, *Nat. Phys.* **2**, 48 (2006).

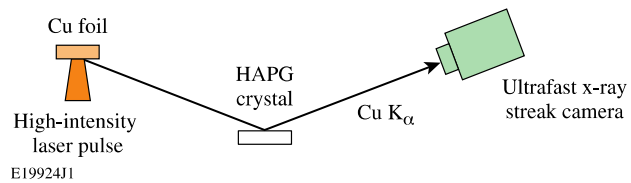


FIG. 1. Experimental setup. HAPG: highly annealed pyrolytic graphite.

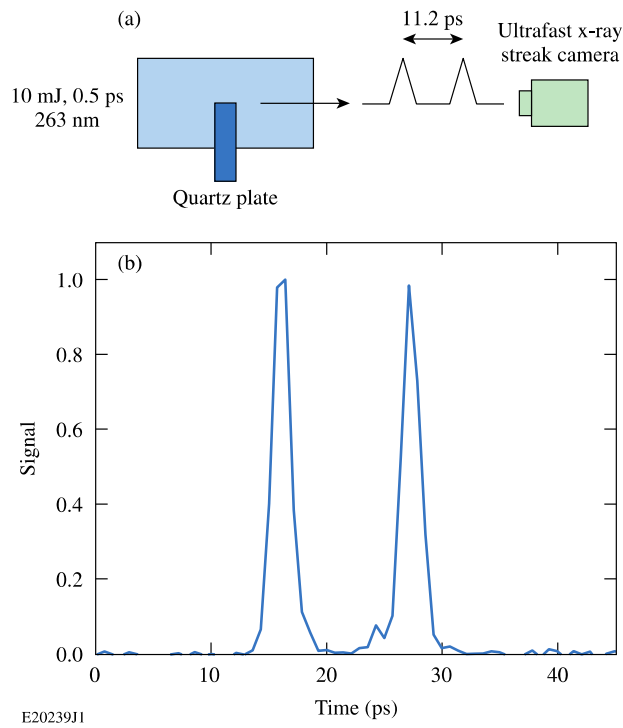


FIG. 2. (a) Streak camera calibration setup. (b) Streak camera response measurement with 0.5-ps, 263-nm pulses showing pulse widths of 1.8 ± 0.1 and 1.9 ± 0.1 ps.

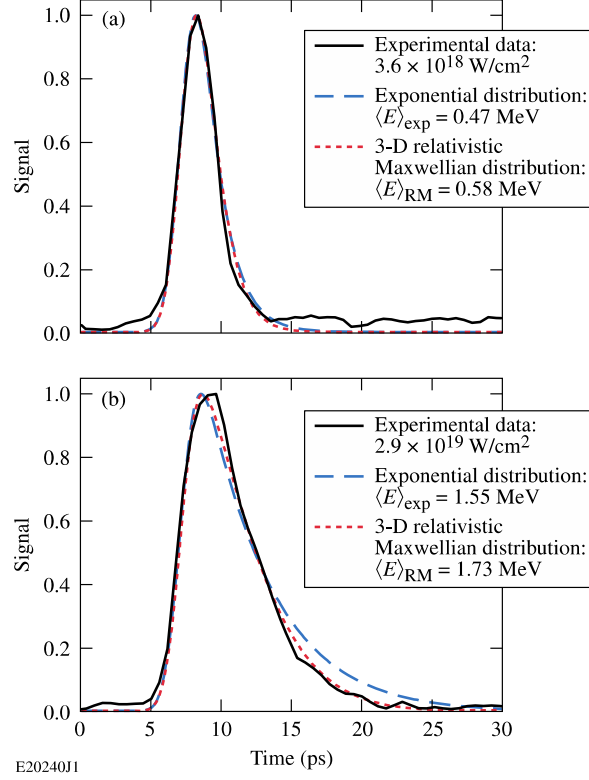


FIG. 3. Experimental time-resolved K_{α} emission data from $500 \times 500 \times 20\text{-}\mu\text{m}^3$ Cu foils. The targets were irradiated with (a) a 0.9-J, 0.6-ps pulse and (b) an 8.7-J, 0.8-ps pulse. The data are shown with theoretical fits based on a collisional energy-loss model with exponential (long-dashed line) and 3-D relativistic Maxwellian (short-dashed line) hot-electron energy distributions.

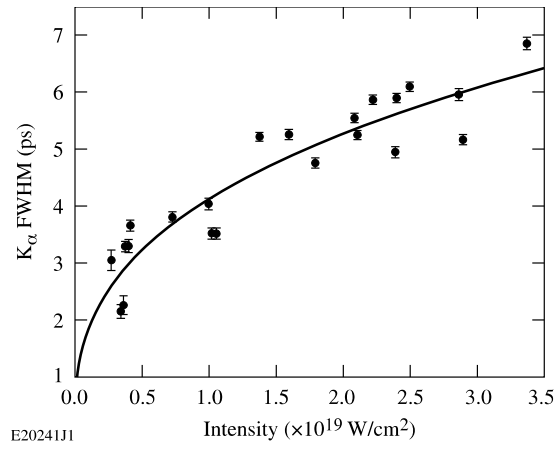


FIG. 4. Experimental K_{α} -emission pulse width as a function of laser intensity. The pulse widths have been adjusted to account for the impulse response of the streak camera.

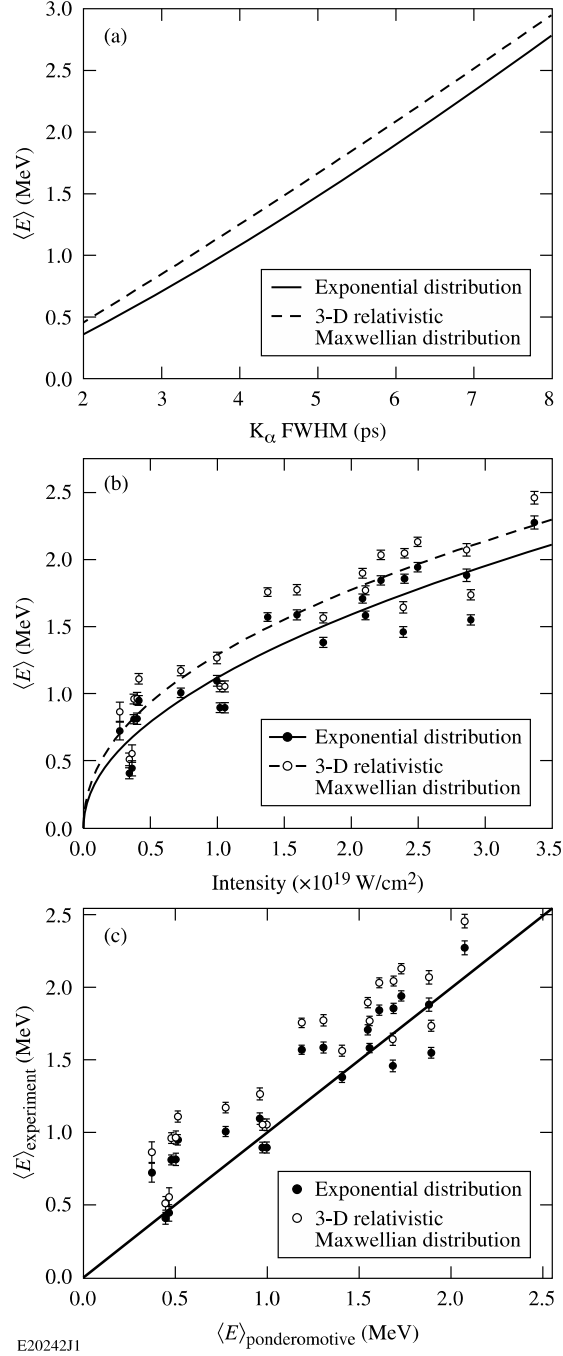


FIG. 5. (a) Calculated mean hot-electron energy $\langle E \rangle$ as a function of K_α -emission pulse width based on a 0.8-ps laser-pulse duration. (b) Inferred $\langle E \rangle$ as a function of laser intensity, assuming exponential (solid line) and 3-D relativistic Maxwellian (dashed line)

hot-electron energy distributions. (c) Comparison of the experimentally inferred $\langle E \rangle$ with ponderomotive scaling [6].